

Isolation of Hypervalent Group-16 Radicals and Their Application in Organic-Radical Batteries

Yasuyuki Imada,[†] Hideyuki Nakano,[‡] Ko Furukawa,^{||} Ryohei Kishi,[§] Masayoshi Nakano,[§] Hitoshi Maruyama,[#] Masaaki Nakamoto,[#] Akira Sekiguchi,[#] Masahiro Ogawa,[⊥] Toshiaki Ohta,[⊥] and Yohsuke Yamamoto^{*,†}

[†]Department of Chemistry, Graduate School of Science, Hiroshima University, Higashi, Hiroshima 739-8526, Japan

[‡]Toyota Central R&D Laboratories, Inc., Nagakute, Aichi 480-1192, Japan

^{||}Center for Instrumental Analysis, Institute for Research Promotion, Niigata University, Niigata 950-2181, Japan

[§]Department of Materials Engineering Science, Graduate School of Engineering Science, Osaka University, Toyonaka, Osaka 560-8531, Japan

[#]Department of Chemistry, Graduate School of Pure and Applied Sciences, University of Tsukuba, Tsukuba, Ibaraki 305-8571, Japan

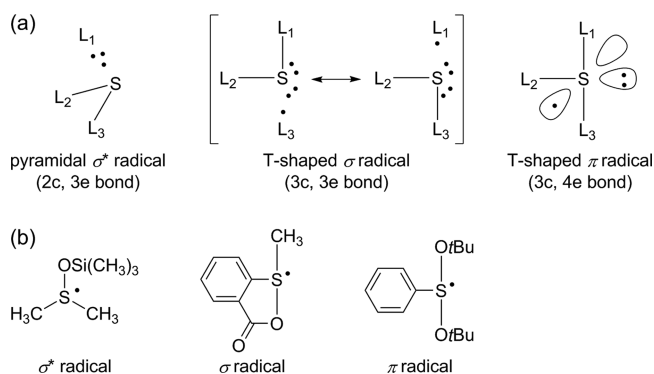
[⊥]SR Center, Ritsumeikan University, Kusatsu, Shiga 525-8577, Japan

Supporting Information

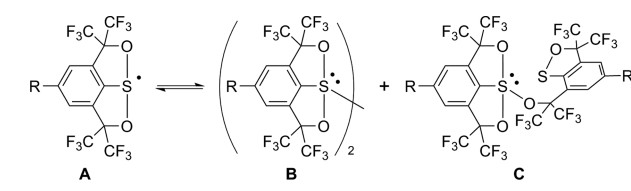
ABSTRACT: Using a newly prepared tridentate ligand, we isolated hypervalent sulfur and selenium radicals for the first time and characterized their structures. X-ray crystallography, electron spin resonance spectroscopy, and density functional theory calculations revealed a three-coordinate hypervalent structure. Utilizing the reversible redox reactions between hypervalent radicals and the corresponding anions bearing Li⁺, we developed organic radical batteries with these compounds as cathode-active materials. Furthermore, an all-radical battery, with these compounds as the cathode and a silyl radical as the anode, was developed that exhibited a practical discharge potential of ~1.8 V and stable cycle performance, demonstrating the potential of these materials for use in metal-free batteries that can replace conventional Li-ion batteries where Li is used in the metal form.

Sulfur-centered radicals are recognized as key intermediates in many biological processes and organic syntheses.¹ Among them, sulfuranyl radicals are considered intermediates in displacement reactions.² They have nine formal valence electrons in their neutral three-coordinate state, giving them a hypervalent structure. The structures of sulfuranyl radicals are categorized into three types: pyramidal σ^* , T-shaped σ , and T-shaped π (Chart 1a).³ The first structure has a two-center, three-electron (2c-3e) bond, whereas the latter two have a three-center, three-electron (3c-3e) bond and a three-center, four-electron (3c-4e) bond, respectively. These structures are experimentally supported by electron spin resonance (ESR) and UV-vis results (Chart 1b).^{3,4} However, no detailed structure elucidation has been reported because they are usually unstable under ambient conditions. In 1986, Martin et al. reported thermally stable sulfuranyl radicals stabilized by a tridentate ligand (Scheme 1, A).⁵ Although these sulfuranyl radicals were reported to be persistent in solution, they existed in equilibrium with dimers B and C⁶ and have not been isolated and structurally characterized

Chart 1. Bonding Types and Examples of Sulfuranyl Radicals



Scheme 1. Thermally Stable Sulfuranyl Radicals (R = H, tBu)



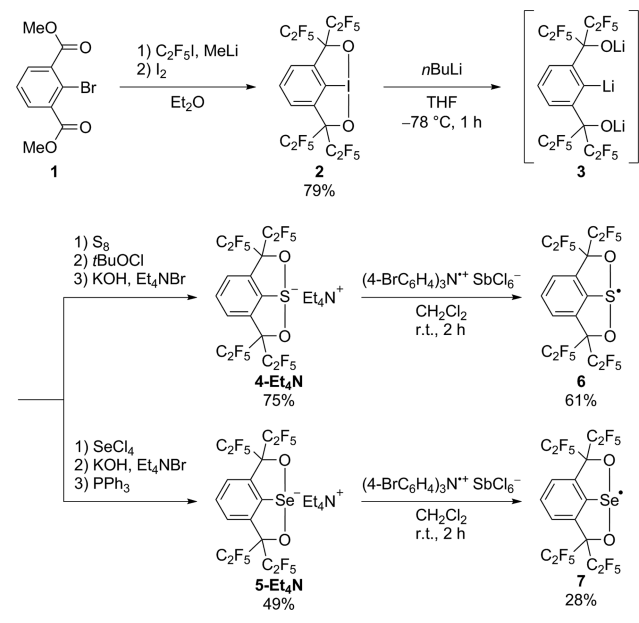
by X-ray analysis. To our knowledge, these radicals are the only examples of stable sulfuranyl radicals, and no further attempts to stably isolate these species have been reported.

We have extensively explored the chemistry of hypervalent compounds containing main-group elements by using various multidentate ligands.⁷ In our study of the fluxional behavior of pentacoordinated phosphorus compounds, we observed that the barrier to isomerization was increased through the use of a bidentate ligand bearing C₂F₅ groups instead of CF₃ groups.^{7b} These results prompted us to examine the synthesis of sulfuranyl radicals stabilized by a bulky tridentate ligand. We envisioned

Received: October 21, 2015

Published: December 31, 2015

Scheme 2. Synthesis of Hypervalent Radicals 6 and 7



that if a tridentate ligand with C_2F_5 groups instead of CF_3 groups was used, dimerization could be inhibited by steric hindrance; thus, sulfuranyl radicals could be isolated as stable monomers, thereby enabling their structural characterization.

Herein, we report the first isolation and structural characterization of stable sulfuranyl radicals and their selenium analogues; these radicals are stabilized by a new tridentate ligand bearing C_2F_5 groups. Furthermore, using the reversible redox reactions between the hypervalent radicals and the corresponding anions, organic radical batteries using these compounds as cathode-active materials were developed. An all-radical battery, with these compounds as the cathode and a silyl radical as the anode, was also developed.

Martin's tridentate ligand was synthesized via a long and complicated synthetic route,⁸ which prevented us from modifying this route to prepare a new C_2F_5 -type tridentate ligand. Thus, we designed and established the simple and efficient synthetic route shown in Scheme 2. Ester 1 was treated with C_2F_5Li , generated *in situ* from C_2F_5I and MeLi, followed by the addition of an excess amount of I_2 to give iodine 2, a tridentate ligand precursor, in 79% yield. Trimetalization of 2 was achieved using *n*-BuLi (3.3 equiv), which was then reacted with electrophiles (S_8 or $SeCl_4$) to give hypervalent anions 4- Et_4N and 5- Et_4N in yields of 75% and 49%, respectively. Cyclic voltammograms of 4- Et_4N and 5- Et_4N showed reversible redox peaks at $E_{1/2} = 0.83$ and 0.81 V (vs SCE), respectively (Figures S8 and S9). Oxidation of sulfur anion 4- Et_4N with 1 equiv of aminium salt ($[4-BrC_6H_4_3N^+ SbCl_6^-]$) in dichloromethane (DCM) at room temperature gave a red crystalline solid of hypervalent sulfur radical 6 in 61% yield. Similarly, selenium radical 7 was obtained from selenium anion 5- Et_4N as an orange crystalline solid in 28% yield.

The molecular structures of radicals 6 and 7 in the solid state were determined by X-ray analysis (Figure 1). No counterions are contained in the unit cells of 6 and 7, indicating that they are neutral species. The crystal structures of 6 and 7 exhibit similar structural features and have slightly asymmetric apical bonds. In 6, the apical S–O bond lengths are 1.723(2) and 2.395(2) Å, which are longer than the sum of the covalent bond radii of S- and O-atoms (1.71 Å) and shorter than the sum of the van der Waals

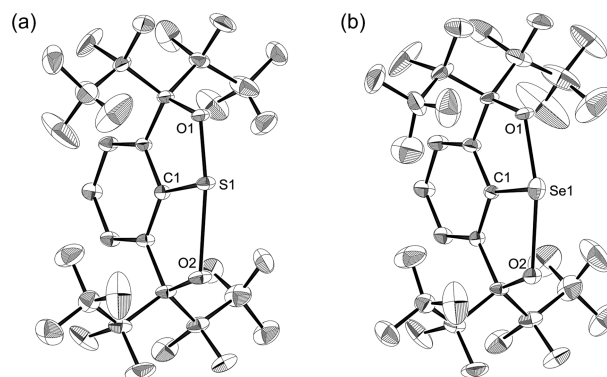


Figure 1. Crystal structures of 6 (a) and 7 (b). Thermal ellipsoids are drawn at the 30% probability level. H-atoms and disorders are omitted for clarity. For 7, two independent molecules exist in the unit cell, but only one is shown. Selected bond lengths (Å) and angles (deg) for 6: S1–O1 = 1.723(2), S1–O2 = 2.395(2), S1–C1 = 1.738(3), O1–S1–O2 = 167.80(9), C1–S1–O1 = 91.98(12), C1–S1–O2 = 75.82(11). Selected bond lengths (Å) and angles (deg) for 7: Se1–O1 = 1.969(4), 1.886(4), Se1–O2 = 2.297(5), 2.382(4), Se1–C1 = 1.870(5), 1.874(5), O1–Se1–O2 = 161.29(15), 161.28(16), C1–Se1–O1 = 84.8(2), 86.6(2), C1–Se1–O2 = 76.5(2), 74.7(2).

(vdW) radii of S- and O-atoms (3.32 Å).⁹ No intermolecular interactions between S-atoms were observed in 6; the closest intermolecular S...S distance is 6.026 Å, far larger than the sum of the vdW radii of two S-atoms (3.70 Å).⁹ However, the intermolecular O...O distance is 2.806 Å, which is equivalent to the sum of the vdW radii of two O-atoms (2.80 Å),⁹ suggesting that intermolecular interactions affect the asymmetric S–O distance (Figure S6). The O1–S1–O2 angle of 167.80(9)° is slightly smaller than the ideal angle between the apical bonds, i.e., 180°. Similarly, in 7, the two apical Se–O bond lengths are nonequivalent; Se1–O1 and Se1–O2 are 1.969(4), 1.886(4) and 2.297(5), 2.382(4) Å (two independent molecules), respectively, which are longer than the sum of the covalent bond radii of Se- and O-atoms (1.83 Å) and shorter than the sum of their vdW radii (3.40 Å).⁹ The smallest Se...Se distance is 6.100 Å, far larger than the sum of the vdW radii of two Se-atoms (4.00 Å);⁹ however, the intermolecular O...O distance is 2.752, 2.747 Å, indicating intermolecular interactions (Figure S7).

Theoretical calculations were carried out to gain further insight into the structure of these radicals. The optimized structure of 6, calculated at the UB3PW91/cc-pVTZ level, is symmetric, with two equivalent S–O bond lengths of 1.819 Å (Figure S12). Differences in the symmetry and the S–O bond lengths of the optimized geometry from those of the X-ray data are considered to originate from packing effects in the crystal. In the atoms-in-molecules (AIM) analysis,¹⁰ bond paths are observed between each S–O bond, and the electron density and Laplacian at the bond critical point (bcp) of the S–O bonds (ρ_{bcp} and $\nabla^2\rho_{bcp}$) are 0.1472, 0.1475 e/a_0^3 and -0.0713 , -0.0726 e/a_0^5 , respectively (Figure S15). Because negative values of $\nabla^2\rho_{bcp}$ imply covalent bond character, the observed negative $\nabla^2\rho_{bcp}$ values of the S–O bonds suggest that they exhibit covalent character, indicating associative interactions. X-ray structure of 6 was also analyzed and shows bond paths between each S–O bond ($\rho_{bcp} = 0.1797$, 0.0439 e/a_0^3 and $\nabla^2\rho_{bcp} = -0.2313$, 0.1072 e/a_0^5), though small ρ_{bcp} and the positive $\nabla^2\rho_{bcp}$ are observed at the longer S–O bond, indicating weak ionic interaction (Figure S16). Furthermore, the spin density distribution of the optimized structure of 6 was calculated (Figure S19), and the largest spin density of

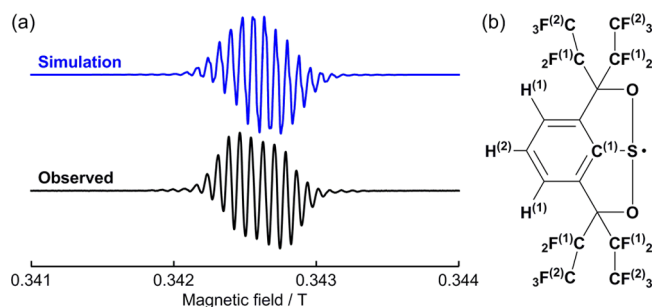


Figure 2. Observed ESR spectrum of **6** in CH_2Cl_2 at room temperature and simulated ESR spectrum with parameters $g = 2.0089$, $A_{\text{H}(1)} = 0.17$ mT, $A_{\text{H}(2)} = 0.07$ mT, $A_{\text{F}(1)} = 0.08$ mT, $A_{\text{F}(2)} = 0.06$ mT, $A_{\text{C}(1)} = 1.27$ mT.

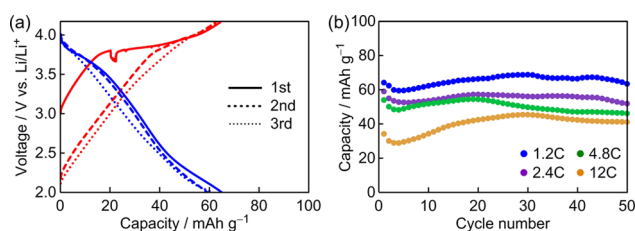


Figure 3. Galvanostatic charge/discharge curves (at 1.2C (0.10 A/g), a) and cycle performance of the discharge processes (at 1.2C, 2.4C, 4.8C, and 12C, b) of the 4-Li cell between 2.0 and 4.2 V vs Li/Li^+ .

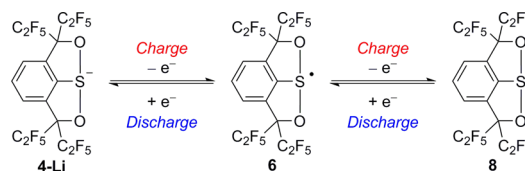
+0.56 observed at the S-atom suggests that **6** is a sulfur-centered radical. Similar calculation results were obtained for **7**, suggesting that **7** is a three-coordinated selenium-centered radical (see SI).

The ESR spectrum of **6** in dichloromethane at room temperature shows a complicated pattern (Figure 2a). That radical **6** remains the sole species in solution was confirmed by comparison with a standard radical substance (Figure S21). This spectrum is reproduced by the hyperfine coupling constant, A , of the proton, the fluorine, and the ^{13}C -atoms, as defined in Figure 2b. These hyperfine coupling constants indicate that **6** has a C_2 -symmetric structure along the $\text{C}^{(1)}\text{--S}$ axis. The spectra observed at the lower temperature (Figure S23) also show a similar coupling pattern, suggesting that **6** has the same symmetry in the ground state. On the other hand, only broad signals were observed in the spectrum of selenium radical **7** (Figure S24).

We subsequently used these hypervalent compounds as cathode-active materials for radical batteries. The Li-ion batteries most commonly employed today use an electrode combination based on a graphite negative electrode¹¹ and a LiCoO_2 ,¹² LiMn_2O_4 ,¹³ or LiFePO_4 ¹⁴ positive electrode. Recently, high-performance organic cathode materials for Li-ion batteries have attracted extensive research interest because of their sustainability, flexibility, and versatile molecular design.¹⁵ However, their use in more demanding applications such as sustainable transport is prevented mainly by the lack of a Li source for use in their cathode materials. To overcome this drawback, as cathode-active materials, we chose anions with a lithium cation (4-Li and 5-Li), which were prepared from 4-Et₄N and 5-Et₄N by counteranion exchange (see SI). To investigate their utility as cathode-active materials, we initially made a coin-type cell composed of a cathode containing 50 wt% of an active material and a Li-metal anode with a porous polymer film separator in an electrolyte solution of 1 M LiPF_6 in 1:1 (v/v) ethylene carbonate/diethyl carbonate.

Figure 3a shows the galvanostatic charge/discharge profiles of the sulfur anion 4-Li cell. The first charge curve exhibited a single

Scheme 3. Redox Mechanism on the Electrode

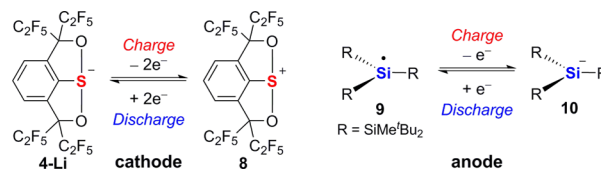


voltage plateau at 3.9 V vs Li/Li^+ , and the subsequent discharge curve exhibited two sloped plateaus at ~ 3.7 and 2.4 V. The first discharge capacity of 64.4 mAh/g is surprisingly larger than the theoretical capacity of a 1-e^- redox process between the anion and the radical (41.5 mAh/g) and is similar to that of a 2-e^- redox process (83.0 mAh/g). The differential capacity curves show two broad peaks during the delithiation (oxidation) and lithiation (reduction) processes that are not observed in the curves for the 1-e^- redox process (Figure S27). A similar situation was observed in the selenium anion 5-Li cell (Figures S25 and S28). Plateaus were observed at 3.7 V in the first charge process and at ~ 3.0 and 2.3 V in the subsequent discharge process. In this case, the first discharge capacity of 76.7 mAh/g is similar to the theoretical capacity of a 2-e^- redox process between the anion and cation (77.4 mAh/g). These larger capacities suggest the involvement of cationic species. For both materials, the plateaus practically disappeared after the second cycle, indicating a structural change to the amorphous phase during the initial oxidation.¹⁶

To investigate the redox mechanism during the electrochemical reactions, we performed ex situ S K-edge XAFS measurements of the electrode of the 4-Li cell upon cycling (Figure S30). In the charge/discharge process, the consecutive spectral changes were observed and were in good agreement with the simulated spectra (see SI). On the basis of these results, we concluded that a cationic species exists and that a stepwise 2-e^- redox reaction between anion 4-Li (at 2.4 V in Figure 3a) and the corresponding cation **8** (at 3.7 V in Figure 3a) occurs, as shown in Scheme 3.

Figure 3b and S26 shows the discharge of 4-Li and 5-Li at various rates after the cells were slowly charged and maintained at 4.2 V to fully charge the material. A rate of $n\text{C}$ corresponds to a full discharge in $1/n$ h. At a 1.2C rate, 4-Li and 5-Li achieve 78% and 99% of their theoretical capacities, respectively (calculated on the basis of a 2-e^- redox process). Even at the highest rate tested (12C), corresponding to a time of 300 s to fully discharge the capacity, these materials achieved 53% and 66% of their theoretical capacities, respectively. After 50 full charge/discharge

Scheme 4. Schematic Description of an All-Radical Battery



cycles at 1.2C and 12C, $\sim 90\%$ of the initial discharge capacities were maintained. In the 4-Li cell, 65% of the discharge capacity at 1.2C was maintained at 12C, whereas 75% was maintained in the 5-Li cell. The differences in these rate properties are attributed to the rate of the redox reaction. With respect to the redox reaction, the selenium anion 5-Li, which exhibited better capacity retention, had a faster reaction rate than the sulfur anion 4-Li.

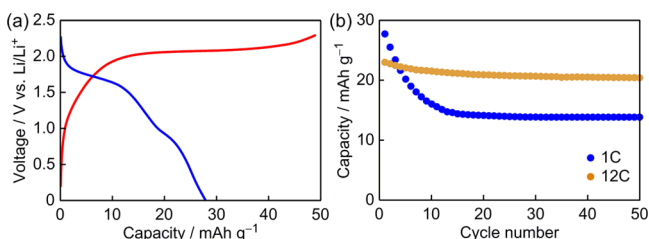


Figure 4. Galvanostatic charge/discharge profiles (a) and cycle performance (b) of the all-radical battery.

For more practical use, we decided to replace the Li-metal anode with organic materials. Examples of fully organic-based batteries in the literature are limited. Nishide and co-workers employed a bipolar radical polymer for both electrodes to create a fully organic-based battery with a working potential of 1.3 V.¹⁷ To develop a fully organic-based battery for our system, we chose a stable persilyl-substituted silyl radical ($t\text{Bu}_2\text{MeSi}$)₃Si[•] (**9**)¹⁸ as an anode-active material (Scheme 4). Cyclic voltammograms of sulfur anion 4-Li and silyl radical **9** display reversible redox processes at $E_{1/2} = 3.7$ and 1.7 V (vs Li/Li⁺, Figures S10 and S11), respectively, and a working potential of ~2 V was expected. Figure 4a shows the charge/discharge curves for the cell with 4-Li and **9**. The charge curve shows a plateau at 2.1 V, and the discharge curve shows a sloped plateau at ~1.8 V, in good agreement with the potential gap between 4-Li and **9**. As shown in Figure 4b, the first discharge capacity at the 1C rate was 27.8 mAh/g, which corresponds to 67% of the theoretical capacity of 4-Li (41.5 mAh/g). The discharge capacity gradually decreased and maintained 50% of the initial value after 50 cycles. However, at 12C, though the first discharge capacity was 23.0 mAh/g, the discharge capacity after 50 cycles was 89% of the initial value. The decrease in the capacity was caused by the dissolution of the sulfur radical into the electrolyte solution. In the case of the cell cycled at 12C, the sulfur radicals were exposed to the electrolyte solution for a shorter time than in the case of the cell cycled at 1C, resulting in better cycle performance.

In summary, we have synthesized, isolated, and structurally characterized hypervalent sulfur and selenium radicals. The reversible redox reaction of the radicals enabled us to apply them in radical batteries. Their useful properties as cathode-active materials were confirmed by electrochemical measurements. An all-radical battery with sulfur anions as the cathode and silyl radicals as the anode exhibited a practical discharge potential of ~1.8 V and stable cycle performance, demonstrating the potential of these materials for use in metal-free batteries that can replace conventional Li-ion batteries where Li is used in the metal form.

ASSOCIATED CONTENT

Supporting Information

The Supporting Information is available free of charge on the ACS Publications website at DOI: 10.1021/jacs.5b10774.

Procedures; characterization data; CVs; XAFS measurements and simulated spectra; charge/discharge curves and differential capacity curves of the cells (PDF)
X-ray crystallographic data (CIF)

AUTHOR INFORMATION

Corresponding Author

*yyama@sci.hiroshima-u.ac.jp

Notes

The authors declare no competing financial interest.

ACKNOWLEDGMENTS

This work was supported by a Grant-in Aid for Science Research on Innovative Areas (No. 24109002, Stimuli-responsive Chemical Species) from the Ministry of Education, Culture, Sports, Science and Technology, Japan. The authors are grateful to Central Glass Co., Ltd., for the generous gift of the iodopentafluoroethane.

REFERENCES

- (1) (a) Gara, W. B.; Roberts, B. P. *J. Organomet. Chem.* **1977**, *135*, C20. (b) Schoneich, C.; Zhao, F.; Madden, K. P.; Bobrowski, K. *J. Am. Chem. Soc.* **1994**, *116*, 4641. (c) Fautitano, A.; Buttava, A.; Mariani, M.; Chatgililoglu, C. *ChemPhysChem* **2005**, *6*, 1100. (d) Kampmeier, J. A.; Hoque, A. M.; Saeva, F. D.; Wedegaertner, D. K.; Thomsen, P.; Ullah, S.; Krake, J.; Lund, T. *J. Am. Chem. Soc.* **2009**, *131*, 10015.
- (2) (a) Pryor, W. A.; Guard, H. *J. Am. Chem. Soc.* **1964**, *86*, 1150. (b) Kampmeier, J. A.; Evans, T. R. *J. Am. Chem. Soc.* **1966**, *88*, 4096. (c) Franz, J. A.; Roberts, D. H.; Ferris, K. F. *J. Org. Chem.* **1987**, *52*, 2256.
- (3) (a) Perkins, C. W.; Martin, J. C.; Arduengo, A. J.; Lau, W.; Alegria, A.; Kochi, J. K. *J. Am. Chem. Soc.* **1980**, *102*, 7753. (b) Chatgililoglu, C.; Castelhan, L.; Griller, D. *J. Org. Chem.* **1985**, *50*, 2516.
- (4) (a) Gara, W. B.; Giles, J. R. M.; Roberts, B. P. *J. Chem. Soc., Perkin Trans. 2* **1979**, 1444. (b) Chapman, J. S.; Cooper, J. W.; Roberts, B. P. *J. Chem. Soc., Chem. Commun.* **1976**, 835.
- (5) Perkins, C. W.; Clarkson, R. B.; Martin, J. C. *J. Am. Chem. Soc.* **1986**, *108*, 3206.
- (6) Perkins, C. W.; Martin, J. C. *J. Am. Chem. Soc.* **1986**, *108*, 3211.
- (7) (a) Akiba, K.-y.; Yamashita, M.; Yamamoto, Y.; Nagase, S. *J. Am. Chem. Soc.* **1999**, *121*, 10644. (b) Jiang, X. D.; Kakuda, K.-i.; Matsukawa, S.; Yamamichi, H.; Kojima, S.; Yamamoto, Y. *Chem. - Asian J.* **2007**, *2*, 314. (c) Yamaguchi, T.; Yamamoto, Y.; Kinoshita, D.; Akiba, K.-y.; Zhang, Y.; Reed, C. A.; Hashizume, D.; Iwasaki, F. *J. Am. Chem. Soc.* **2008**, *130*, 6894.
- (8) Nguyen, T. T.; Amey, R. L.; Martin, J. C. *J. Org. Chem.* **1982**, *47*, 1024.
- (9) Emsley, J. *The Elements*, 3rd ed.; Oxford University Press: Oxford, 1998.
- (10) Bader, R. F. W. *Atoms in Molecules—A Quantum Theory*; Oxford University Press: Oxford, 1990.
- (11) (a) Aurbach, D.; Markovsky, B.; Weissman, I.; Levi, E.; Ein-Eli, Y. *Electrochim. Acta* **1999**, *45*, 67. (b) Aurbach, D.; Markovsky, B.; Shechter, A.; Ein-Eli, Y.; Cohen, H. *J. Electrochem. Soc.* **1996**, *143*, 3809.
- (12) (a) Cho, J.; Kim, Y. J.; Park, B. *Chem. Mater.* **2000**, *12*, 3788. (b) Amatucci, G. G.; Tarascon, J. M.; Klein, L. C. *Solid State Ionics* **1996**, *83*, 167.
- (13) (a) Tarascon, J. M.; Wang, E.; Shokoohi, F. K.; McKinnon, W. R.; Colson, S. *J. Electrochem. Soc.* **1991**, *138*, 2859. (b) Kim, D. K.; Muralidharan, P.; Lee, H.-W.; Ruffo, R.; Yang, Y.; Chan, C. K.; Peng, H.; Huggins, R. A.; Cui, Y. *Nano Lett.* **2008**, *8*, 3948.
- (14) (a) Malik, R.; Zhou, F.; Ceder, G. *Nat. Mater.* **2011**, *10*, 587. (b) Yamada, A.; Chung, S. C.; Hinokuma, K. *J. Electrochem. Soc.* **2001**, *148*, A224.
- (15) (a) Armand, M.; Grugeon, S.; Vezin, H.; Laruelle, S.; Ribière, P.; Poizot, P.; Tarascon, J.-M. *Nat. Mater.* **2009**, *8*, 120. (b) Morita, Y.; Nishida, S.; Murata, T.; Moriguchi, M.; Ueda, A.; Satoh, M.; Arifuku, K.; Sato, K.; Takui, T. *Nat. Mater.* **2011**, *10*, 947.
- (16) Kim, J.; Manthiram, A. *Nature* **1997**, *390*, 265.
- (17) Suga, T.; Sugita, S.; Ohshiro, H.; Oyaizu, K.; Nishide, H. *Adv. Mater.* **2011**, *23*, 751.
- (18) Maruyama, H.; Nakano, H.; Nakamoto, M.; Sekiguchi, A. *Angew. Chem., Int. Ed.* **2014**, *53*, 1324.